GAṆANAM (गणनम्)

HIGH PERFORMANCE *COMPUTING* NEWSLETTER

INSTITUTE FOR PLASMA RESEARCH, INDIA

INSIDE THIS ISSUE
(4 Pages)

Effect of radiation-reaction on charged particle dynamics in ultra-intense laser light

Dr. Shivam Kumar Mishra (Post Doctoral Fellow, BTSD, IPR)
Email: shivam.mishra@ipr.res.in

Laser technology has seen remarkable advancements over the past few decades. The chirped pulse amplification (CPA) technique, recognized with the Nobel Prize in Physics in 2018, has enabled the delivery of intensities on the order of 10^{23}W/cm^2 (electric fields on the order of 10^{13}V/cm). Such strong electromagnetic (EM) fields can accelerate electrons to ultra-relativistic energies (~ GeV) in a fraction of the time compared to the period of the laser [1]. This offers a more convenient and cost-effective alternative for particle acceleration compared to conventional accelerators. Consequently, exploring the dynamics of charged particles in such high fields is of significant contemporary interest for both theoretical research and technological applications.

It is well known that an accelerating charged particle radiates energy irreversibly that affect the dynamics of the charged particle by providing a self-influence called the self-force or radiationreaction (RR) force. RR force significantly affects the charged particle dynamics when the power radiated by the particle becomes comparable to the instantaneous rate of change of mechanical energy of the particle. For an electron with an energy of ~1GeV moving in a femtosecond laser with a focused intensity of ~10^{22}W/cm^2 , the RR force may becomes comparable to the Lorentz force [1]. In this scenario, the Lorentz force equation is not an appropriate choice for investigating the charged particle dynamics. The Hartemann-Luhmann (HL) equation (see equation (1)) in one of equation of motion for charged particle which, within the framework of classical electrodynamics, self-consistently takes into account the effect of RR forces.

$$\dot{u}^\alpha = \frac{e}{mc}F^{\alpha\beta}u_\beta + \tau_0 \frac{\dot{u}^\beta \dot{u}_\beta}{c^2}u^\alpha$$

[Equation 1]

Here $F^{\alpha\beta}$ is the EM field tensor. $u^\alpha = (\gamma c, \vec{p})$ is the four-velocity with $\gamma = \sqrt{1+p^2}$ (where $\vec{p}$,c, e, and m are the momentum of the particle, the speed of light, the charge on an electron, and the mass of an electron respectively), and dot represents derivative with respect to proper time t. We use the metric convention (+1, -1,-1,-1). To the best of our knowledge, the HL equation has no known solutions for the motion of a charged particle in any EM field configurations other than uniform magnetic and electric fields. The covariant form of the HL equation of motion is in an implicit form, where acceleration becomes a nonlinear function of itself, and no explicit form of the HL equation (where acceleration is a function of particle position, velocity, and external force fields) exists. As a result, finding an exact solution of the HL equation for a charged particle in ultra-relativistic, intense focused lasers becomes impractical, and a numerical approach is required. A MATLAB-based 3-D test particle code has been developed to solve the HL equation for any arbitrary field configuration. Particularly, the dynamics of the charged particle in the focused laser light has been studied [2]. For our numerical work, the initial conditions are chosen in such a way that, without RR, the particle reflects back from the focused regime. The normalization are used

$$t \to \omega t,\ \vec{r} \to k\vec{r},\ F^{\alpha\beta} \to eF^{\alpha\beta}/(mc\omega) \text{ and } \vec{p} \to \vec{p}/(mc)$$

(here ω and k are the frequency and wave vector of the EM wave). The results are shown in the figure (1). These all the simulations (for HL equation) are performed using the ANTYA-HPC facility at IPR. The runtime of simulation is approximately 1 hours for 16 cores of ANTYA-HPC Cluster.

We now present results obtained for a charged particle interacting with a linearly polarized, intense, focused wave train. We first discuss the particle dynamics in the absence of RR effects. In sub-figures (1) (a)-(c), the red and green curves, respectively represent the forward and the reflected motion of the particle in the absence of RR effects (values correspond to y-axis on the left). The red curves in sub-figure (1) (a) and (b) respectively show that as the particle approaches the focal point (increasing laser intensity), the average longitudinal momentum (momentum along the wave propagation direction) decreases monotonically and approaches zero, whereas the amplitude of the transverse momentum simultaneously increases. After reflection (represented by the green curves), as the particle moves away from the focal point (decreasing laser intensity), the absolute value of average longitudinal momentum increases and the particle leaves the focal region with a finite value of longitudinal momentum in the opposite direction, whereas the amplitude of the transverse momentum decreases and eventually goes to zero. The corresponding energy is shown in sub-figure (1) (c), which shows that for our choice of parameters the average energy which remains with the particle after reflection is around γ ~ 600 (~ 0.3GeV). Finally, sub-figure (1) (d) shows the evolution of the parameter $\Delta = \gamma - p_z$ as a function of z coordinate, which continuously increases throughout the motion as shown by the red curve. The green curve on top of the red curve is a plot of the analytical expression of Δ, which clearly shows an excellent match with the numerical result.

For the same set of initial conditions, in the presence of RR effects the particle dynamics which is now governed by the Hartemann-Luhmann equation (values correspond to y-axis on the right), exhibit dramatic changes. (See the blue curve in sub-figures (1) (a), (c) and (d)). Initially when the RR effects are weak, the average longitudinal momentum $\overline{p_z}$ remains almost constant (see blue curve in sub-figure (1) (a); in fact it shows a slight decrease, which is in agreement with the behaviour governed by the Lorentz force equation, and later increases monotonically when the RR term starts dominating over the Lorentz force term. This dominance of the RR term over the Lorentz force term can also be seen from the evolution of the parameter Δ (see sub-figure (1)(d)) which shows that Δ which was initially increasing, starts monotonically decreasing when the intensity becomes sufficiently large (intensity ~ 4×10^{23}W/cm^2) which happens when the particle reaches around z ~ -0.6*10^4. From this location onwards, the RR term starts dominating over the Lorentz force term. Simultaneously, from around the same location i.e. z ~ -0.6*10^4 , the average longitudinal momentum begins to increase monotonically and the particle eventually passes through the focal point with a finite amount of longitudinal momentum. The transverse momentum on the other hand shows a behaviour which is similar to the earlier case, i.e.when RR effects are absent or weak . The amplitude of the transverse momentum of the particle increases as it approaches the focal point and diminishes as it passes through the focal point, eventually becoming zero as it exits the focal region (see blue curve in sub-figure (1)(b)). Therefore the final energy gain as seen in sub-figure (1)(c) (blue curve), is entirely due to the net gain in longitudinal momentum [2-3]. According to this, in the RR dominated regime, a monotonic decrease in the parameter Δ implies energy gain along with increase in forward longitudinal momentum. The energy gain is found to be γ ~ 1.4*10^4 (~ 7GeV) which is two orders of magnitude higher than the earlier case. In conclusion, the dynamics is primarily governed by two effects viz. ponderomotive effects due to focussing and RR forces. The monotonic decrement in value of Δ shows dominance of RR on pondermotive force. Our results clearly show that irrespective of the choice of initial conditions, in the presence of RR, the particle does not reflect from the focal region (provided RR force dominates over Lorentz force), thereby gaining a large amount of energy and forward momentum from the focused laser light [2].

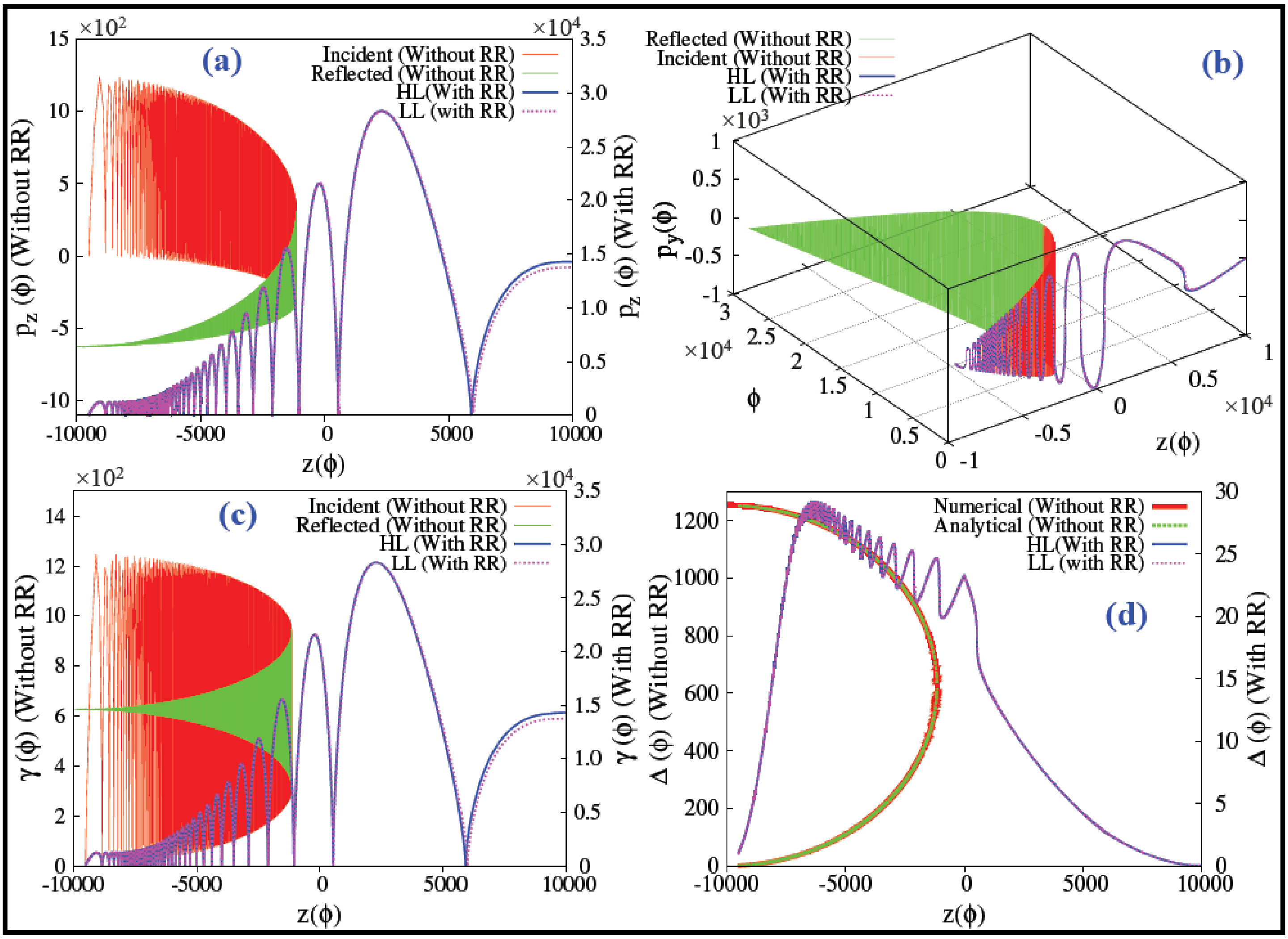

FIG. 1. (a) - (d) respectively represent the evolution of longitudinal momentum (p_z) and transverse momentum ($p_\perp$), the energy and the parameter Δ, for a charged particle interacting with a linearly polarized, intense, focused EM wave, in the absence / presence of RR effects. The intensity at the focal point is chosen as ~10^{24}W/cm^2 and $T_0 \approx$ 1.8*10^{-8}. The initial conditions are z_0 = -9500, $\vec{p}$ = 0. The red and green curves in sub-figures (a) - (c) respectively represent the forward and reflected motion of the particle in the absence of RR effects (values correspond to y-axis on the left), and the corresponding value of the parameter Δ is represented in sub-figure (d) where the red and green curve respectively represent the numerical values and the analytical expression for Δ. The blue and magenta curves in the sub-figures (a) - (d) respectively represent the dynamics in the presence of RR effects (values correspond to y-axis on the right) as governed by HL and LL equation of motion.

References:

1. Mishra S. K. et al, Eur. Phys. J. Spec. Top., 230(23): 4165-4174, (2021).
2. Mishra S. K. et al, Scientific Reports, 12(1):19263, (2022).
3. Mishra S. K. et al, Phys. Plasmas, 31, 043106 (2024).

Introduction to CUDA Libraries: Part 2

In this series, we are looking at 1D complex-to-complex transform applied to the input data. FFT Transformation. The following snippet explains the code from here, wherein code efficiently performs FFT using CUDA's CUFFT library with O (NlogN) complexity, leveraging GPU parallelism for speed. It features in-place transformations to minimize memory usage, custom normalization kernels for flexibility, and non-blocking CUDA streams to overlap computation with data transfer. Error handling macros ensure robustness, and proper resource management prevents memory leaks.

```
##Declares a pointer d_data for device data. Creates the CUFFT plan. Plans a 1D
   FFT with the specified size and batch size.

cufftComplex *d_data = nullptr;    CUFFT_CALL(cufftCreate(&plan));
CUFFT_CALL(cufftPlan1d(&plan, fft_size, CUFFT_C2C, batch_size));

## Creates a non-blocking CUDA stream and associates it with the CUFFT plan.

CUDA_RT_CALL(cudaStreamCreateWithFlags(&stream, cudaStreamNonBlocking));
CUFFT_CALL(cufftSetStream(plan, stream));

## This allocates memory on the device for d_data and copies the data from the host
   to the device asynchronously.

CUDA_RT_CALL(cudaMalloc(reinterpret_cast<void **>(&d_data), sizeof(data_type) *
 data.size()));
CUDA_RT_CALL(cudaMemcpyAsync(d_data, data.data(), sizeof(data_type) *
 data.size(), cudaMemcpyHostToDevice, stream));

##This executes a forward CUFFT in-place transform (complex-to-complex).
CUFFT_CALL(cufftExecC2C(plan, d_data, d_data, CUFFT_FORWARD));

## Calls a kernel scaling kernel to normalize the data (assumed to be defined
   elsewhere).
scaling_kernel<<<1, 128, 0, stream>>>(d_data, element_count, 1.f/fft_size);

## Executes an inverse CUFFT in-place transform (complex-to-complex) to recover
   the originaldata.
CUFFT_CALL(cufftExecC2C(plan, d_data, d_data, CUFFT_INVERSE));

## Copies the data back from the device to the host
CUDA_RT_CALL(cudaMemcpyAsync(data.data(), d_data, sizeof(data_type) *
data.size(), cudaMemcpyDeviceToHost, stream));

CUDA_RT_CALL(cudaStreamSynchronize(stream));

## free resources & destroys stream/plan
CUDA_RT_CALL(cudaFree(d_data))
CUFFT_CALL(cufftDestroy(plan));
CUDA_RT_CALL(cudaStreamDestroy(stream));
CUDA_RT_CALL(cudaDeviceReset());
 return EXIT_SUCCESS; }
```

INPUT ARRAY	Output Array after Forward FFT, Normalization and Inverse FFT
0.000000 + 0.000000j	0.000000 + 0.000000j
1.000000 + -1.000000j	0.125000 + -0.125000j
2.000000 + -2.000000j	0.250000 + -0.250000j
3.000000 + -3.000000j	0.375000 + -0.375000j
4.000000 + -4.000000j	0.500000 + -0.500000j
5.000000 + -5.000000j	0.625000 + -0.625000j
6.000000 + -6.000000j	0.750000 + -0.750000j
7.000000 + -7.000000j	0.875000 + -0.875000j
8.000000 + -8.000000j	1.000000 + -1.000000j
9.000000 + -9.000000j	1.125000 + -1.125000j
10.000000 + -10.000000j	1.250000 + -1.250000j

ANTYA UPDATES AND NEWS

1. New Packages/Applications Installed

To check the list of available modules
$ module avail –l

HPC PICTURE OF THE MONTH

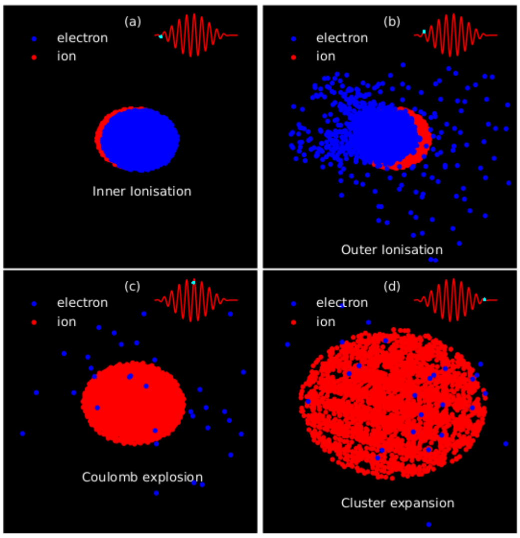

Pic Credit: Kalyani Swain

Coulomb explosion is a well-known phenomenon in laser-cluster interactions. (a) When a high-intensity laser beam interacts with a nano-cluster target, it ionizes the cluster constituents (Inner ionization), creating a cloud of charged particles. (b) As the laser intensity increases, electrons start leaving the cluster boundary (Outer ionization), and the Coulomb repulsion between the ions becomes pronounced. (c) Eventually, the repulsive forces overcome the binding forces, leading to a rapid expansion of the ionic background (Coulomb explosion) results into (d) the expansion of cluster (Cluster expansion).

We simulate the interaction of a 10-cycle laser pulse (intensity of 7.13×10^16 W/cm² and wavelength of 800 nm) with a 3.3 nm cluster containing 7208 particles using a C++-based 3D particle-in-cell (PIC) code in the ANTYA Linux cluster at IPR. Post-simulation data analysis the visualization is conducted using MATLAB, and the visualization is created using Python.

ANTYA Utilization: JULY 2024

ANTYA Daily Observed Workload

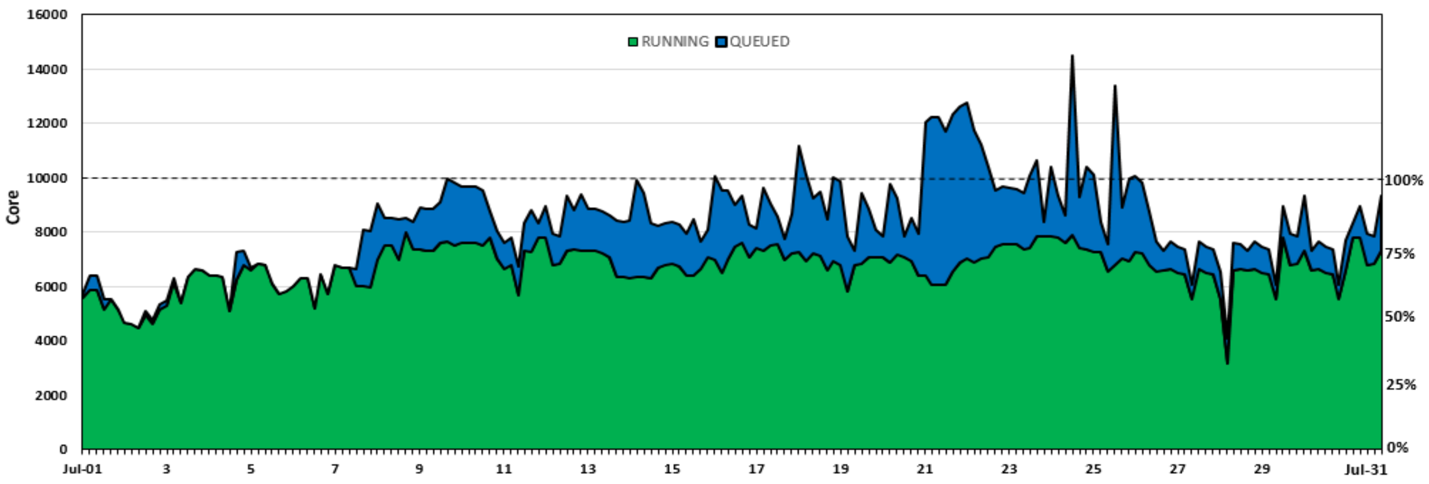

Other Recent Work on HPC

Development and testing of novel hybrid CICC joint	Piyush Raj
High temperature superconducting magnet for magnetic fusion: R&D update and plan	Upendra Prasad
Design, fabrication, installation and testing of a cold bore vertical cryostat for High temperature superconducting magnets	Mahesh M Ghate
ईटर टोकामक भवन की दक्षिणी दीवार में प्रस्तावित भारी परमाणु द्वार के लिए विकिरण परिवहन गणना और टोकामक भवन की दक्षिणी दीवार के बाहर स्वीकार्य विकिरण प्राप्त करने के	Jyoti Agarwal
Design, Simulation, and Testing of Wave Collection and Transport System for Michelson Interferometer Diagnostic	Abhishek Sinha
Design and Performance analysis of Reconfigurable	Manisha Jha
Study of the effect of Plasma Carburizing process on tribological properties of Titanium alloy	Ghanshyamsinh Ranjitsinh Jhala
Real-time UAV Detection through RF Signal Analysis	Rana Pratap Yadav
Exploration of geometric parameters of Pillow plate panel for heat transfer and pressure drop criteria for the cryogenic application	Hemang S. Agravat
Nonlinear Mode Coupling in a 1D Dusty Plasma	Ankit Dhaka

ANTYA HPC USERS' STATISTICS— JULY 2024

Total Successful Jobs~ 1600

- **CPU Cores** — Amit Singh
- **GPU Cards** — Suruj Kalita
- **Walltime** — Amit Singh
- **Jobs** — Suruj Kalita

Acknowledgement

The HPC Team, Computer Division IPR, would like to thank all Contributors for the current issue of *GAṆANAM*.

On Demand Online Tutorial Session on HPC Environment for New Users Available
Please send your request to ***hpcteam@ipr.res.in.***

Join the HPC Users Community
hpcusers@ipr.res.in
If you wish to contribute an article in GAṆANAM, please write to us.

Contact us
HPC Team
Computer Division, IPR
Email: ***hpcteam@ipr.res.in***